

Multiport Atom Interferometry for Inertial Sensing

Dimitry Yankelev,^{1,2,*} Chen Avinadav,^{1,2,*} Nir Davidson,¹ and Ofer Firstenberg¹

¹*Department of Physics of Complex Systems, Weizmann Institute of Science, Rehovot 7610001, Israel*

²*Rafael Ltd, Haifa 3102102, Israel*

We present new techniques for inertial-sensing atom interferometers which produce multiple phase measurements per experimental cycle. With these techniques, we realize two types of multiport measurements, namely quadrature phase detection and real-time systematic phase cancellation, which address challenges in operating high-sensitivity cold-atom sensors in mobile and field applications. We confirm experimentally the increase in sensitivity due to quadrature phase detection in the presence of large phase uncertainty, and demonstrate suppression of systematic phases on a single shot basis.

Cold atom interferometers have demonstrated extremely high sensitivity as inertial sensors measuring gravity [1–3], gravity gradients [4–8], accelerations and rotations [9–17]. In addition to precision measurements of physical constants [18–22], tests of general relativity [23–28], searches for dark energy [29, 30], and gravitational wave detection [31, 32], they are promising candidates as on-board inertial measurement units [10, 33–35] and as mobile gravimeters for geodesic studies or subterranean exploration [36–41]. These prospects provide strong motivation for improving the robustness of atom interferometers while maintaining high phase sensitivity and accuracy under field conditions, such as strong vibrations and drifts in the thermal and magnetic environment.

Atom interferometers typically yield a single phase measurement per shot. This may limit their performance in challenging conditions: first, phase sensitivity is maximal in the linear regime near mid-fringe, which requires locking the phase from shot to shot [40]. This is difficult to maintain when the inertial signal changes on short timescales, such as in mobile applications, or when vibrations introduce large uncontrolled phase variation. Real-time correction using classical sensors can be applied to return the interferometer to mid-fringe [40, 42], but effects such as delay in their response [43] ultimately limit their effectiveness for strong vibrations. Second, many systematic phase shifts are typically canceled with the “ k -reversal” technique, using sequential measurements with opposite wave vectors [5, 44]. However, it is not effective against fast variations in systematic effects, which may arise in field applications, and it inherently reduces the bandwidth and sensitivity per $\sqrt{\text{Hz}}$ of the interferometer.

In this Letter, we introduce two new schemes which extend inertial-sensing atom interferometers to yield multiple phase signals in each experiment, increasing its information bandwidth and improving its performance. One scheme utilizes a composite beam-splitter, which replaces the final beam-splitter in typical atom interferometers, and the other is based on operating dual concurrent interferometers on a single atomic ensemble, with independent control of their phases. Using these schemes, we demonstrate two measurement approaches which address chal-

lenges of deployable atom interferometers. The first approach realizes quadrature phase detection, maintaining peak sensitivity at all phases and avoiding low-sensitivity shots away from mid-fringe. The second approach uses concurrent k -reversal interferometry for real-time cancellation of systematic phase shifts.

Atom interferometers based on stimulated two-photon Raman transitions [45, 46] use two atomic states separated by momentum and internal state, e.g. $|1, 0\rangle \equiv |F=1, p=0\hbar k\rangle$ and $|2, 2\rangle \equiv |F=2, p=2\hbar k\rangle$, where k is the wave vector of the Raman lasers. In the following we consider the Mach-Zehnder sequence with three Raman pulses $\pi/2$ - π - $\pi/2$ equally separated by time T [1]. The first beam-splitter pulse generates a coherent superposition of $|1, 0\rangle$ and $|2, 2\rangle$ which then spatially drift apart, followed by a mirror pulse which redirects them back towards each other. The final beam-splitter mixes the states coherently and produces interference in their populations, which constitute the output ports of the interferometer. Its phase in this sequence is $\phi = \mathbf{k}_{\text{eff}} \cdot \mathbf{a}T^2$ where $\mathbf{k}_{\text{eff}} \cong 2\mathbf{k}$ is the effective wave vector of the Raman interaction and \mathbf{a} the relative acceleration between the atoms and the mirror reflecting the Raman beams. For a gravimeter this simplifies to $\phi_{\text{grav}} = k_{\text{eff}}gT^2$. Our multiport interferometry schemes exploit the momentum degree of freedom to produce additional output signals with different phases and extract more information from each experiment cycle.

In the first scheme, a composite beam-splitter replaces the final beam-splitter pulse with a combination of microwave rotations, state-dependent light shifts, and narrowband Raman transition. This operation couples two additional states, $|1, 2\rangle$ and $|2, 0\rangle$ [Fig. 1(a)], whose interference contrast and phase is determined by the pulse parameters of the composite beam-splitter. We numerically found such values, depicted in Fig. 1(a), which produce two pairs of interference signals in phase quadrature.

Conversely, the concurrent interferometry scheme relies on initializing the atomic ensemble in two different momentum states of the same ground state and applying the interferometric pulse-sequence to both states simultaneously, resulting in four output ports. By independently controlling the phase and frequency of the nar-

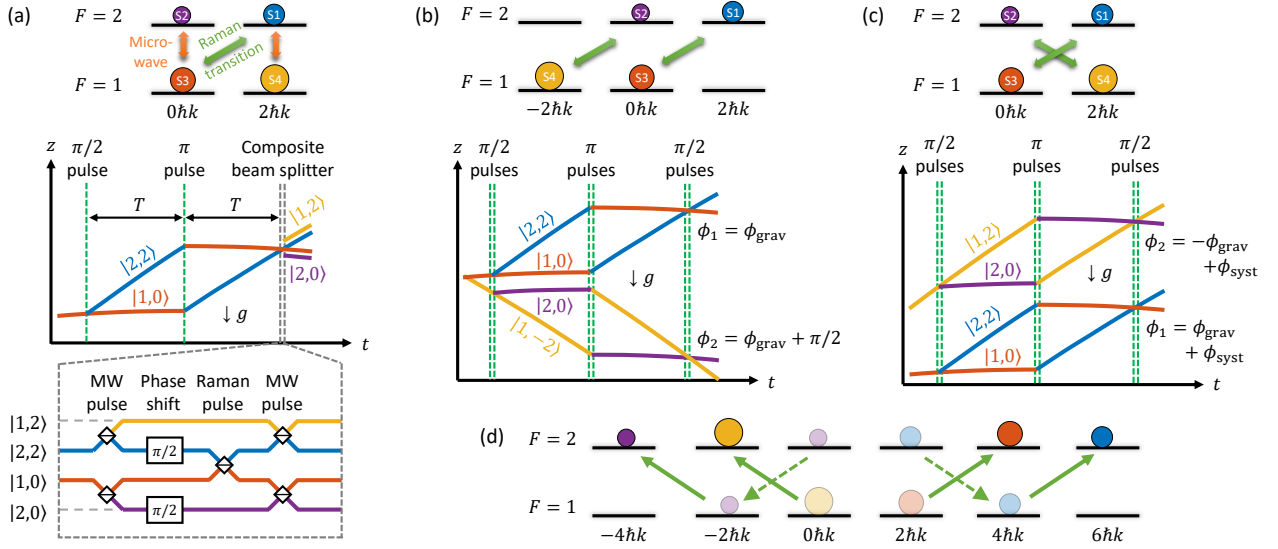


Figure 1. Multipoint interferometry and detection. (a) Quadrature detection with composite beam-splitter. The composite operation (inset) consists of a $\pi/3$ microwave pulse, a $\pi/2$ differential phase shift, a narrowband 0.6π Raman pulse, and a final $\pi/2$ microwave pulse, resulting in $\pi/2$ phase difference between the interference in states $|1, 0\rangle$, $|2, 2\rangle$ and $|1, 2\rangle$, $|2, 0\rangle$. S_i represent fractional populations in the four relevant states, in arbitrary order. (b) Quadrature detection with concurrent interferometry. Atoms are initialized in an equal mixture of $|1, 0\rangle$ and $|1, -2\rangle$, which undergo simultaneous Raman transitions. The relative phase between the Raman fields is changed by $\pi/2$ before the final beam-splitter pulse. (c) Real-time k -reversal with concurrent interferometry. Initial states are $|1, 0\rangle$ and $|1, 2\rangle$, and the two Raman transitions are tuned to impart opposite momentum kicks. (d) Example of multipoint detection scheme. Dashed arrows represent shelving of $F = 2$ populations in $F = 1$ followed by blow-away, solid arrows represent sequential promotions to $F = 2$, each followed by resonant fluorescent detection and blow-away. This example corresponds to detection of interferometers (a) and (c); detection of (b) differs only in some shelving and promotion operations.

rowband Raman pulses which address each momentum state, we realize different types of multipoint measurements: quadrature detection, where the phase of the Raman pulses differs by $\pi/2$ on the final beam-splitter pulse [Fig. 1(b)]; and k -reversal, where the frequency of the Raman pulses is chirped in opposite directions to address opposite momentum transitions [Fig. 1(c)], changing the sign of ϕ_{grav} but not the sign of many systematic phases, denoted collectively as ϕ_{sys} [44].

Measuring the multiple output ports in either scheme requires velocity- and state-dependent detection. Constrained by small spatial separation of the output states, we use a combination of velocity-selective Raman pulses and state-selective resonant detection. Following the interferometry sequence, $F = 2$ populations are first transferred to empty momentum states in $F = 1$. Then, sequentially, each momentum state is transferred to $F = 2$, where it is counted and blown away by a resonant light pulse [Fig. 1(d)].

Both multipoint schemes are compatible with many Raman atom interferometers, including different pulse sequences such as $\pi/2$ - π - π - $\pi/2$ for rotation sensing [10–13] and large momentum transfer interferometers [47, 48]. Interferometers operating in micro-gravity [33], where atoms are scattered into multiple momentum states due

to vanishing Doppler shift [?], may also benefit from multipoint interferometry and detection. Concurrent interferometry should also be compatible with zero-dead-time and interleaved operation [13]. Comparing the two multipoint schemes, the composite beam-splitter has the advantage that all output ports result from a single interferometer loop and fundamentally measure the same inertial phase, whereas the concurrent interferometer does not require stabilized light-shift pulses or microwave rotations, and allows for more versatile multipoint configurations such as k -reversal. Previous applications of concurrent atom interferometers were limited to gravity gradiometers, which are inherently insensitive to inertial forces, or to Ramsey-Bordé interferometers [49–51] in measurements of the fine-structure constant. Quadrature detection was previously realized using two different atomic species to operate two interferometers [52], which adds experimental complexity and is susceptible to uncommon noise sources of the two species.

Our apparatus prepares an ensemble of $\sim 10^8$ ^{87}Rb atoms at $\sim 6\ \mu\text{K}$ and launches it upwards at velocities of up to 1.5 m/s using moving optical molasses. Retro-reflected Raman beams with σ^+/σ^+ polarizations traverse the system vertically and interact with the atoms along their trajectory for initialization, interferometry,

and multipoint detection. The Raman mirror is placed on a vibration isolation platform whose residual vibrations are measured using a classical accelerometer. The Raman beams originate from a 780 nm DBR laser, locked 700 MHz below the $F = 2 \rightarrow F' = 1$ transition and passing through a fiber electro-optic modulator (EOM) and a semiconductor optical amplifier. The Raman beams have 40 mm $1/e^2$ diameter and a total power of 200 mW in all sidebands. For simultaneous addressing of two velocity classes in concurrent interferometry, the EOM microwave signal contains two spectral components independently generated by a direct digital synthesizer and up-shifted to approximately 6.834 GHz using a single-sideband mixer. A horizontal beam resonant with $F = 2 \rightarrow F' = 3$ is used for blow-away and fluorescence detection.

The atoms initially populate all Zeeman sublevels of the $F = 2$ manifold and have a thermal momentum distribution with $\sim 9\hbar k$ FWHM. Narrowband Raman pulses select atoms from $m_F = 0$ with a momentum spread of $0.7\hbar k$ FWHM. For the composite beam-splitter, the selection is centered on the mean ensemble momentum \bar{p} , while for concurrent interferometry, we select two groups at $\bar{p} \pm \hbar k$. The latter is possible due to the wide thermal distribution; a colder ensemble could be initialized in two different momentum or hyperfine states by microwave, Raman, or Bragg transitions. The interferometer pulses have a bandwidth of $1.1\hbar k$ FWHM, which allows addressing the velocity-selected states with high fidelity and minimal cross-talk between states separated by $2\hbar k$.

The state-dependent phase-shift for the composite beam-splitter is implemented with a laser beam detuned 1 GHz below the $F = 2 \rightarrow F' = 3$ transition, inducing a differential light shift between $F = 1$ and $F = 2$. The pulse duration and power are first calibrated using standard Raman-interferometry to create the necessary $\pi/2$ phase shift. This pulse has similar duration, detuning and intensity as the interferometer Raman pulses and thus additional scattering is insignificant.

We characterize the multipoint detection sequence by selecting atoms in one momentum state, performing standard Mach-Zehnder interferometry, and measuring the population of all four output ports. As Fig. 2(a) shows, high-contrast fringes are measured in the expected output states with little cross-talk between the pairs, demonstrating the high fidelity of our detection scheme. Such measurements can be used to calibrate the detection process transformation and correct its imperfections.

A demonstration of quadrature detection using both composite beam-splitter and concurrent interferometry schemes is shown in Fig. 2(b-c). The four output signals in both cases are in nearly perfect quadrature. We analyze quadrature measurements by taking the differential population of each pair of signals and fitting an ellipse to their Lissajous curve. Once the ellipse fit is known, we estimate the phase for each individual measurement

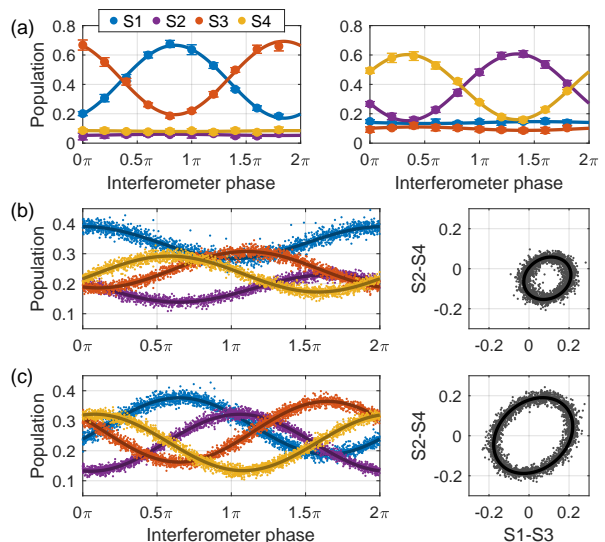


Figure 2. (a) Characterization of multipoint detection. Four output ports measured following a standard interferometer sequence, when populating only the initial states $|1, 0\rangle$ (left) or $|1, -2\rangle$ (right). The cross-talks, measured by the contrast ratios between the initially unpopulated and populated states, are $(1.4 \pm 0.8)\%$ and $(3.9 \pm 1.2)\%$ respectively. Solid lines are least-squares fringe fits. (b) Four output signals in the composite beam-splitter scheme (left) and their representation as an ellipse in a Lissajous plot (right). The contrast ratio between the quadrature fringes is 1.11 and their relative phase 0.45π . The Raman laser phase was scanned randomly over 2π . (c) Same as (b) for the concurrent interferometry scheme. The contrast ratio here is 1.04 and the relative phase 0.42π . Mean contrast is 70% higher than for the composite beam-splitter due to the lack of additional microwave and light shift operations. Data measured with $2T = 2$ ms.

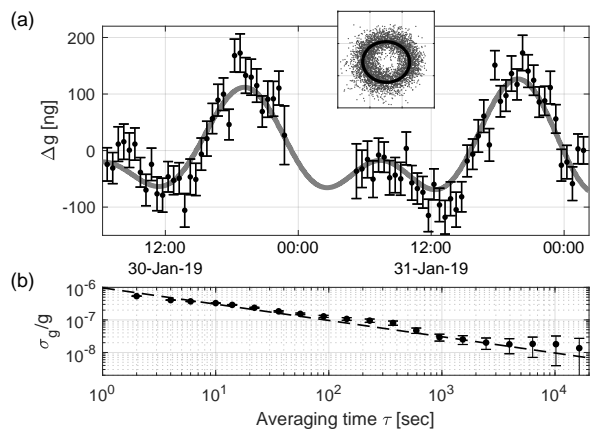


Figure 3. Sensitivity and long-term stability of concurrent quadrature interferometry. (a) Gravity variations measured over 44 hours with $2T = 140$ ms. Inset shows raw data over several hours. Time is in UTC, data points are averaged over 30-minute bins, solid line is the tidal model calculated at the measurement site (Haifa, Israel). (b) Allan deviation of gravity measurements after subtracting the tidal model. Dashed line is a fit to $\tau^{-1/2}$.

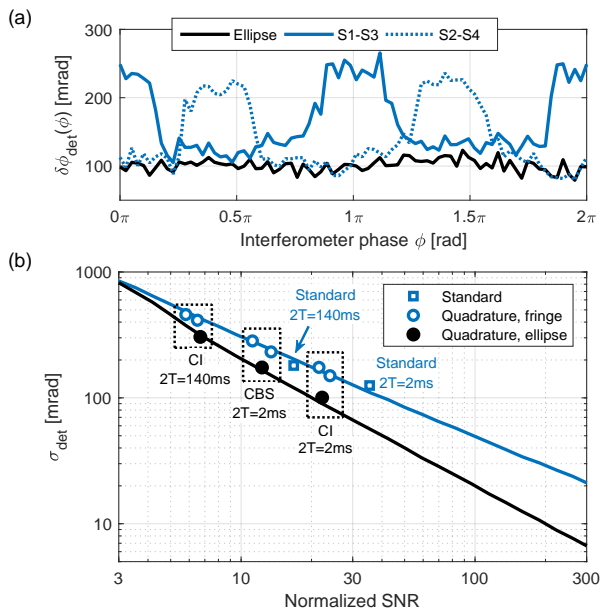


Figure 4. Analysis of phase sensitivity. (a) Standard deviation of phase uncertainty due to detection noise $\delta\phi_{\text{det}}$, as a function of the interferometer phase ϕ for concurrent interferometry with $2T = 2$ ms, using ellipse analysis of all output ports (black) or single-fringe analysis of each pair separately (blue). Results extracted from 14,000 measurements. (b) Overall phase uncertainty σ_{det} as a function of normalized SNR for ellipse analysis (black) and single-fringe analysis (blue). Markers represent experimental results at several conditions, with the SNR estimated from the measured data. Lines represent numerical simulations. “Standard” stands for regular two-port interferometry, CI is concurrent interferometry, and CBS is composite beam-splitter. Cloud expansion at longer T lowers the fidelity of the Raman pulses and consequently decreases the SNR.

from the nearest point on the ellipse.

We test the performance of quadrature detection by realizing concurrent interferometry with $2T = 140$ ms and measuring gravity variations over 44 hours (Fig. 3). The results follow the expected changes due to gravity tides, and residuals from the tidal model indicate a sensitivity of $0.96 \mu\text{g}/\sqrt{\text{Hz}}$, consistent with technical noise sources in our apparatus, and stability of 13 ng at 1.6×10^4 sec. The measurements presented in Fig. 2(b-c) also maintained stability for the duration of the run (6 and 15 hours respectively; data not shown). This demonstrates the compatibility of our quadrature detection method for high-sensitivity operation and its long-term stability.

We now turn to a detailed analysis of the improved phase sensitivity of quadrature versus standard fringe detection. We consider a single interferometric signal, $S = A - \frac{C}{2} \cos(\phi + \delta\phi) + \delta S$, where A and C are the fringe offset and contrast, ϕ the interferometer phase, $\delta\phi \sim N(0, \sigma_\phi)$ represents laser phase noise or imperfect vibration correction [53], and $\delta S \sim N(0, \sigma_S)$ is detec-

tion noise with signal-to-noise ratio (SNR) of C/σ_S . σ_S and σ_ϕ can be estimated from the measurement noise at fringe extrema and mid-fringe, respectively. The total phase uncertainty is given by $\delta\phi_{\text{tot}} = \delta\phi_{\text{det}} + \delta\phi$, with $\delta\phi_{\text{det}}$ the uncertainty from a single data point due to finite SNR. $\delta\phi_{\text{det}}$ depends not only on σ_S but also on ϕ itself, with its variance being minimal near mid-fringe and maximal near its extrema. Conversely, in ellipse analysis of quadrature signals this term is independent of ϕ and equals to the mid-fringe uncertainty of single-fringe analysis with the same SNR. We demonstrate this experimentally in Fig. 4(a), clearly highlighting the advantage of quadrature detection when the interferometer phase varies far from mid-fringe.

To quantify the performance of quadrature detection, we estimate the overall phase uncertainty due to SNR, denoted as σ_{det} , from measurements where the phase varies randomly over 2π . Assuming independent detection and phase noises, we have $\sigma_{\text{det}}^2 = \sigma_{\text{tot}}^2 - \sigma_\phi^2$, with σ_{tot}^2 the two-sample Allan variance of the estimated phase. We present the results in Fig. 4(b) for the two quadrature schemes (concurrent interferometry and composite beam-splitter) and for standard two-port interferometry, at various SNR values and interrogation times T . We observe good agreement with the numerical simulations of the two detection schemes. For additional validation of the simulations, we also present the single-fringe analysis of the quadrature measurements. Notably, quadrature detection outperforms standard fringe detection at any given SNR. The relative sensitivity gain increases with increasing SNR, e.g. from 1.5 to 2.5 for SNR values from 10 to 100. Consequently, reduction in SNR due to implementation of quadrature detection becomes less significant at higher SNR values.

Finally, we present proof-of-principle demonstration of concurrent interferometry for real-time systematic phase-shift cancellation using k -reversal. In these experiments, we control the inertial phase by changing the chirp rate of the Raman lasers [44], and we simulate systematic phase shifts by adding a light-shift pulse to the interferometer and varying its power. As expected, we find the relative phase between pairs of opposite- k fringes corresponds to the inertial phase, whereas their common phase corresponds to the systematic effect (Fig. 5). We observe that even for large systematic contributions of 2π , we extract the same inertial phase up to $33 \text{ mrad}(1\sigma)$. This indicates a lower bound for the suppression ratio of 190:1, likely limited by SNR in these measurements. Contrary to traditional sequential implementation of the k -reversal technique, the method presented here allows evaluation of both inertial and systematic phases from a single shot of the experiment by measuring the multiple ports of the interferometer.

In conclusion, we introduce new techniques that bring multipoint detection capabilities to inertial-sensing atom interferometers. The two techniques, a compos-

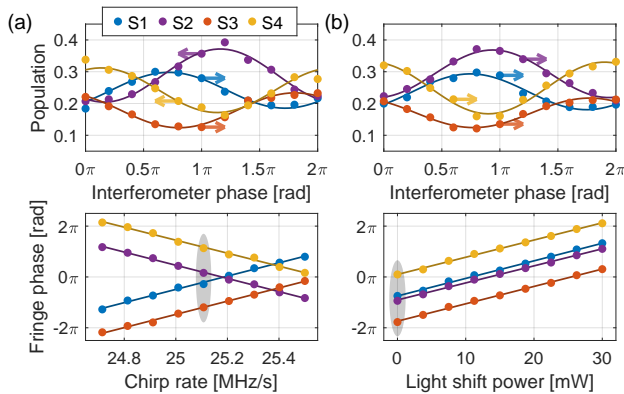


Figure 5. Concurrent k -reversal interferometry. (a) Top: Raw output signals measured for a specific value of the Raman chirp rate. Bottom: The fringe phases of each output port as a function of chirp rate. As the chirp rate changes, representing a change in the measured acceleration, the two pairs of fringes shift in opposite directions and their relative phase is linearly proportional to the applied chirp. Shaded points in bottom figure correspond to the fringes shown above. (b) Same as (a), but as a function of the light-shift pulse power, simulating different systematic shifts, at a fixed chirp rate. In this case, all fringes shift in the same direction and their relative phase remains stable despite the changing systematic phase. Data measured with $2T = 4$ ms.

ite beam-splitter and concurrent interferometry, increase the phase information measured per experimental cycle. We demonstrate two applications of multiport interferometry: quadrature phase detection, which maintains constant and high phase sensitivity and bandwidth in the presence of large phase variations, and real-time k -reversal, capable of measuring and canceling systematic effects even as they change on fast timescales. Both applications are expected to increase the performance and robustness of future quantum inertial sensors operating in challenging field conditions, in the face of large and uncontrolled phase variations and noisy environments. The methods presented in this paper can be readily extended to additional output ports, e.g. 6- or 8-port interferometers. For example, advanced sensors based on dual-wavelength interferometers, e.g., 780 and 795 nm, with dramatically increased dynamic range due to their different scale factors, would require quadrature detection to avoid phase ambiguities.

We thank Yoav Erlich and Igal Levy for technical assistance. This work was supported by the Pazy Foundation.

* These authors contributed equally to this work. Electronic addresses: dimitry.yankelev@weizmann.ac.il, chen.avinadav@weizmann.ac.il.

[1] M. Kasevich and S. Chu, *Physical Review Letters* **67**,

181 (1991).

- [2] A. Peters, K. Y. Chung, and S. Chu, *Nature* **400**, 849 (1999).
- [3] A. Peters, K. Y. Chung, and S. Chu, *Metrologia* **38**, 25 (2001).
- [4] M. Snadden, J. McGuirk, P. Bouyer, K. Haritos, and M. Kasevich, *Physical Review Letters* **81**, 971 (1998).
- [5] J. M. McGuirk, G. T. Foster, J. B. Fixler, M. J. Snadden, and M. A. Kasevich, *Physical Review A* **65** (2002), 10.1103/physreva.65.033608.
- [6] F. Sorrentino, A. Bertoldi, Q. Bodart, L. Cacciapuoti, M. de Angelis, Y.-H. Lien, M. Prevedelli, G. Rosi, and G. M. Tino, *Applied Physics Letters* **101**, 114106 (2012).
- [7] F. Sorrentino, Q. Bodart, L. Cacciapuoti, Y.-H. Lien, M. Prevedelli, G. Rosi, L. Salvi, and G. M. Tino, *Physical Review A* **89** (2014), 10.1103/physreva.89.023607.
- [8] G. W. Biedermann, X. Wu, L. Deslauriers, S. Roy, C. Mahadeswaraswamy, and M. A. Kasevich, *Physical Review A* **91** (2015), 10.1103/physreva.91.033629.
- [9] B. Barrett, R. Geiger, I. Dutta, M. Meunier, B. Canuel, A. Gauguier, P. Bouyer, and A. Landragin, *Comptes Rendus Physique* **15**, 875 (2014).
- [10] B. Canuel, F. Leduc, D. Holleville, A. Gauguier, J. Fils, A. Viridis, A. Clairon, N. Dimarcq, C. J. Bordé, A. Landragin, and P. Bouyer, *Physical Review Letters* **97** (2006), 10.1103/physrevlett.97.010402.
- [11] J. K. Stockton, K. Takase, and M. A. Kasevich, *Physical Review Letters* **107** (2011), 10.1103/physrevlett.107.133001.
- [12] B. Wu, Z. Wang, B. Cheng, Q. Wang, A. Xu, and Q. Lin, *Metrologia* **51**, 452 (2014).
- [13] D. Savoie, M. Altorio, B. Fang, L. A. Sidorenkov, R. Geiger, and A. Landragin, *Science Advances* **4**, eaau7948 (2018).
- [14] T. L. Gustavson, P. Bouyer, and M. A. Kasevich, *Physical Review Letters* **78**, 2046 (1997).
- [15] S. M. Dickerson, J. M. Hogan, A. Sugarbaker, D. M. S. Johnson, and M. A. Kasevich, *Physical Review Letters* **111** (2013), 10.1103/physrevlett.111.083001.
- [16] G. W. Hoth, B. Pelle, S. Riedl, J. Kitching, and E. A. Donley, *Applied Physics Letters* **109**, 071113 (2016).
- [17] Y.-J. Chen, A. Hansen, G. W. Hoth, E. Ivanov, B. Pelle, J. Kitching, and E. A. Donley, *arXiv* **1812.00106** (2018).
- [18] D. S. Weiss, B. C. Young, and S. Chu, *Physical Review Letters* **70**, 2706 (1993).
- [19] J. B. Fixler, G. T. Foster, J. M. McGuirk, and M. A. Kasevich, *Science* **315**, 74 (2007).
- [20] R. Bouchendira, P. Cladé, S. Guellati-Khélifa, F. Nez, and F. Biraben, *Physical Review Letters* **106** (2011), 10.1103/physrevlett.106.080801.
- [21] G. Rosi, F. Sorrentino, L. Cacciapuoti, M. Prevedelli, and G. M. Tino, *Nature* **510**, 518 (2014).
- [22] R. H. Parker, C. Yu, W. Zhong, B. Estey, and H. Müller, *Science* **360**, 191 (2018).
- [23] S. Dimopoulos, P. W. Graham, J. M. Hogan, and M. A. Kasevich, *Physical Review Letters* **98** (2007), 10.1103/physrevlett.98.111102.
- [24] K.-Y. Chung, S. wey Chiow, S. Herrmann, S. Chu, and H. Müller, *Physical Review D* **80** (2009), 10.1103/physrevd.80.016002.
- [25] H. Müller, A. Peters, and S. Chu, *Nature* **463**, 926 (2010).
- [26] M. A. Hohensee, S. Chu, A. Peters, and H. Müller,

- Physical Review Letters **106** (2011), 10.1103/physrevlett.106.151102.
- [27] D. N. Aguilera, H. Ahlers, B. Battelier, A. Bawamia, A. Bertoldi, R. Bondarescu, K. Bongs, P. Bouyer, C. Braxmaier, L. Cacciapuoti, C. Chaloner, M. Chwalla, W. Ertmer, M. Franz, N. Gaaloul, M. Gehler, D. Gerardi, L. Gesa, N. Gürlebeck, J. Hartwig, M. Hauth, O. Hellmig, W. Herr, S. Herrmann, A. Heske, A. Hinton, P. Ireland, P. Jetzer, U. Johann, M. Krutzik, A. Kubelka, C. Lammerzahn, A. Landragin, I. Lloro, D. Massonnet, I. Mateos, A. Milke, M. Nofrarias, M. Oswald, A. Peters, K. Posso-Trujillo, E. Rasel, E. Rocco, A. Roura, J. Rudolph, W. Schleich, C. Schubert, T. Schuldt, S. Seidel, K. Sengstock, C. F. Sopuerta, F. Sorrentino, D. Summers, G. M. Tino, C. Trenkel, N. Uzunoglu, W. von Klitzing, R. Walser, T. Wendrich, A. Wenzlawski, P. Wessels, A. Wicht, E. Wille, M. Williams, P. Windpassinger, and N. Zahzam, *Classical and Quantum Gravity* **31**, 115010 (2014).
- [28] L. Zhou, S. Long, B. Tang, X. Chen, F. Gao, W. Peng, W. Duan, J. Zhong, Z. Xiong, J. Wang, Y. Zhang, and M. Zhan, *Physical Review Letters* **115** (2015), 10.1103/physrevlett.115.013004.
- [29] P. Hamilton, M. Jaffe, P. Haslinger, Q. Simmons, H. Müller, and J. Khoury, *Science* **349**, 849 (2015).
- [30] M. Jaffe, P. Haslinger, V. Xu, P. Hamilton, A. Upadhye, B. Elder, J. Khoury, and H. Müller, *Nature Physics* **13**, 938 (2017).
- [31] P. W. Graham, J. M. Hogan, M. A. Kasevich, and S. Rajendran, *Physical Review Letters* **110** (2013), 10.1103/physrevlett.110.171102.
- [32] B. Canuel, A. Bertoldi, L. Amand, E. P. di Borgo, T. Chantreau, C. Danquigny, M. D. Álvarez, B. Fang, A. Freise, R. Geiger, J. Gillot, S. Henry, J. Hinderer, D. Holleville, J. Junca, G. Lefèvre, M. Merzougui, N. Mielec, T. Monfret, S. Pelisson, M. Prevedelli, S. Reynaud, I. Riou, Y. Rogister, S. Rosat, E. Cormier, A. Landragin, W. Chaibi, S. Gaffet, and P. Bouyer, *Scientific Reports* **8** (2018), 10.1038/s41598-018-32165-z.
- [33] R. Geiger, V. Ménotet, G. Stern, N. Zahzam, P. Cheinet, B. Battelier, A. Villing, F. Moron, M. Lours, Y. Bidel, A. Bresson, A. Landragin, and P. Bouyer, *Nature Communications* **2** (2011), 10.1038/ncomms1479.
- [34] X. Wu, F. Zi, J. Dudley, R. J. Bilotta, P. Canoza, and H. Müller, *Optica* **4**, 1545 (2017).
- [35] P. Cheiney, L. Fouché, S. Templier, F. Napolitano, B. Battelier, P. Bouyer, and B. Barrett, *Physical Review Applied* **10** (2018), 10.1103/physrevapplied.10.034030.
- [36] X. Wu, *Gravity Gradient Survey with a Mobile Atom Interferometer*, Ph.D. thesis, Stanford (2009).
- [37] K. Bongs, J. Malcolm, C. Ramelloo, L. Zhu, V. Boyer, T. Valenzuela, J. Maclean, A. Piccardo-Selg, C. Meller, T. Fernholz, M. Fromhold, P. Krüger, O. Hellmig, A. Grote, S. Dörscher, H. Duncker, P. Windpassinger, K. Sengstock, C. Becker, B. Pelle, A. Hilico, M. Zhou, M.-C. Angonin, P. Wolf, F. P. D. Santos, F. Bertoldi, P. Bouyer, T. Mazzoni, N. Poli, F. Sorrentino, M. Tarallo, G. M. Tino, S. Stellmer, F. Schreck, M. Popp, W. Herr, T. Wendrich, W. Ertmer, E. Rasel, C. Kürbis, A. Peters, and A. Wicht, in *Research in Optical Sciences* (OSA, 2014).
- [38] C. Freier, M. Hauth, V. Schkolnik, B. Leykauf, M. Schilling, H. Wziontek, H.-G. Scherneck, J. Müller, and A. Peters, *Journal of Physics: Conference Series* **723**, 012050 (2016).
- [39] Y. Bidel, N. Zahzam, C. Blanchard, A. Bonnin, M. Cadoret, A. Bresson, D. Rouxel, and M. F. Lequentrec-Lalancette, *Nature Communications* **9** (2018), 10.1038/s41467-018-03040-2.
- [40] V. Ménotet, P. Vermeulen, N. Le Moigne, S. Bonvalot, P. Bouyer, A. Landragin, and B. Desruelle, *Scientific Reports* **8**, 12300 (2018).
- [41] L. Zhu, *A cold atoms gravimeter for use in absolute gravity comparisons*, Ph.D. thesis, University of Birmingham (2018).
- [42] J. Lautier, L. Volodimer, T. Hardin, S. Merlet, M. Lours, F. P. D. Santos, and A. Landragin, *Applied Physics Letters* **105**, 144102 (2014).
- [43] S. Merlet, J. L. Gouët, Q. Bodart, A. Clairon, A. Landragin, F. P. D. Santos, and P. Rouchon, *Metrologia* **46**, 87 (2009).
- [44] A. Louchet-Chauvet, T. Farah, Q. Bodart, A. Clairon, A. Landragin, S. Merlet, and F. P. D. Santos, *New Journal of Physics* **13**, 065025 (2011).
- [45] M. Kasevich, D. S. Weiss, E. Riis, K. Moler, S. Kasapi, and S. Chu, *Physical Review Letters* **66**, 2297 (1991).
- [46] K. Moler, D. S. Weiss, M. Kasevich, and S. Chu, *Physical Review A* **45**, 342 (1992).
- [47] J. M. McGuirk, M. J. Snadden, and M. A. Kasevich, *Physical Review Letters* **85**, 4498 (2000).
- [48] K. Kotru, D. L. Butts, J. M. Kinast, and R. E. Stoner, *Physical Review Letters* **115** (2015), 10.1103/physrevlett.115.103001.
- [49] S. wey Chiow, S. Herrmann, S. Chu, and H. Müller, *Physical Review Letters* **103** (2009), 10.1103/physrevlett.103.050402.
- [50] B. Estey, C. Yu, H. Müller, P.-C. Kuan, and S.-Y. Lan, *Physical Review Letters* **115** (2015), 10.1103/physrevlett.115.083002.
- [51] W. Zhong, R. H. Parker, Z. Pagel, C. Yu, and H. Müller, *arXiv* **1901.03487** (2019).
- [52] A. Bonnin, C. Diboune, N. Zahzam, Y. Bidel, M. Cadoret, and A. Bresson, *Applied Physics B* **124** (2018), 10.1007/s00340-018-7051-5.
- [53] We assume Gaussian noise in the discussion for simplicity.